

The Surprising Anisotropy of Fast Rotating, Disky Elliptical Galaxies

Andreas Burkert and Thorsten Naab

University Observatory Munich, Scheinerstr. 1, D-81679 Munich, Germany

Submitted to MNRAS

ABSTRACT

The projected kinematical properties of unequal-mass merger remnants of disk galaxies are analysed and shown to agree well with observations of disk, fast rotating elliptical galaxies. This supports the major merger hypothesis of early-type galaxy formation. However, in contrast to previous claims, the merger remnants are very anisotropic with values of the anisotropy parameter that are similar to equal-mass merger remnants that form boxy, slowly rotating ellipticals. Including gas in the simulations does not change this result although the line-of-sight velocity profile and the intrinsic orbital structure are strongly affected by the presence of gas. The kinematical difference between boxy and disk ellipticals appears not to be the amount of anisotropy but rather rotation and the shape of the velocity dispersion tensor. The apparent isotropy of observed disk ellipticals is shown to result from inclination effects. Even small inclination angles strongly reduce the measured anisotropy of fast rotating systems, seen in projection. A second problem is the limited amount of information that is available when measuring only the central velocity dispersion and a characteristic rotation and ellipticity. Methods are investigated that allow a better determination of the intrinsic anisotropy of fast rotating early-type galaxies with known inclination angles.

Key words: galaxies: ellipticals – galaxies: formation – galaxies: evolution

1 INTRODUCTION

Elliptical galaxies are old stellar systems that are believed to have formed from major mergers of disk galaxies, preferentially at high redshifts (Searle, Sargent & Bagnuolo 1973; Toomre & Toomre 1972). This “merger hypothesis” has been tested using numerical simulations (e.g. Gerhard 1981, Neogroponte & White 1983, Barnes 1988). Early simulations demonstrated consistently that merger remnants can account for many characteristic global properties of ellipticals, like their surface density profiles (Trujillo et al. 2004), ellipticities, sizes and large velocity dispersions.

More recently it has however become clear that early-type galaxies are more complex than originally thought. Isophotal fine structures have been detected that correlate well with kinematical properties (Bender et al. 1989). Faint ellipticals are fast rotators with small minor axis rotation. They are called disk as a Fourier analyses of their isophotal deviations from perfect ellipses leads to positive values of the fourth order Fourier coefficient a_4 . In contrast, bright ellipticals are in general boxy with negative values of a_4 and slow rotation. The importance of anisotropy has been es-

timated using the so called anisotropy parameter (Binney 1978)

$$\left(\frac{v}{\sigma}\right)^* = \frac{v/\sigma}{\sqrt{\epsilon/(1-\epsilon)}}, \quad (1)$$

where v is a characteristic rotational velocity, σ is the central velocity dispersion, and ϵ is the ellipticity. Disky ellipticals have values of $(v/\sigma)^* \geq 0.7$ and therefore are believed to be rotationally flattened, isotropic stellar systems. Boxy ellipticals, on the other hand, are characterized by $(v/\sigma)^* << 1$, indicating that they are flattened by an anisotropic velocity dispersion.

In order to understand the origin of boxy and disk ellipticals and their kinematical properties within the framework of the major merger scenario many simulations have been performed (Hernquist 1992, 1993; Naab, Burkert & Hernquist 1999; Bendo & Barnes 2000; González-García & van Albada 2003; Nipotti, Londrillo & Ciotti 2003; for recent reviews see Burkert & Naab 2004a,b). Naab & Burkert (2003) presented a large parameter survey of disk galaxy mergers with statistically unbiased orbital initial conditions and different mass ratios η of the progenitors. They showed

that unequal mass 3:1 and 4:1 mergers lead to fast rotating, disk systems, in good agreement with the observations of disk ellipticals. Equal-mass mergers, on the other hand, tend to form slowly rotating, boxy ellipticals. 2:1 mergers generate a mixed population of boxy and disk systems. Most massive ellipticals are boxy, while 2/3 of the lower-mass ellipticals are disk (Bender, Burstein & Faber 1992). This observation is at first not expected within the framework of a scenario where the isophotal shape depends mainly on the mass ratio η of the merging galaxies as cosmological models predict that the distribution of η is independent of galaxy mass (Khochfar & Burkert 2005). Khochfar & Burkert (2005) however showed that the observations can be reconciled with theory if mixed mergers between ellipticals and spirals and elliptical-elliptical mergers are taken into account (see also González-García & Balcells 2005) which dominate for high masses and produce boxy, anisotropic remnants, independent of η .

In summary, a consistent picture of early-type galaxy formation is emerging and theoretical investigations are now focussing on a more detailed understanding of star formation and energetic feedback processes during major mergers (Bekki 1999, Mihos & Hernquist 1996, Meza et al. 2003; Cox et al. 2005). A particularly interesting recent study in this context is the growth of central black holes or AGN feedback and its effect on the gaseous and stellar environment (Merrifield 2004; Springel, Di Matteo & Hernquist 2005; Di Matteo, Springel & Hernquist 2005) Although feedback is treated very simplified, these models can successfully reproduce the tight correlation between the mass of central black holes and the velocity dispersion of the stellar component (Ferrarese & Merritt 2000; Gebhardt et al. 2000; Tremaine et al. 2002).

Despite all of this progress a still unsolved puzzle is the apparent isotropy of fast rotating, disk ellipticals. Major mergers disturb kinematically cold, rotationally supported disk galaxies enough to generate kinematically hot spheroidal stellar components. They should also destroy any initially isotropic velocity distribution, leading at the end to anisotropic systems. Two-body relaxation which drives the systems towards an isotropic velocity distribution is not efficient in ellipticals because of their long relaxation timescales that by far exceed the age of the Universe. In addition, Dehnen & Gerhard (1994) showed that the line-of-sight velocity dispersions of fast rotating ellipticals are not consistent with isotropic rotator models. Why then do observed ellipticals appear isotropic and how does their hidden anisotropy differ from that of boxy, slowly rotating ellipticals?

It is this question which we plan to investigate in this paper. Section 2 summarizes some important stellar dynamical relations and definitions, following the recent work of Binney (2005). Section 3 investigates the distribution of observed ellipticals in the anisotropy diagram. Section 4 demonstrates that unequal-mass mergers with and without gas lead to fast rotating ellipticals that are however very anisotropic in apparent conflict with the observations. In section 5 inclination effects are investigated which can reconcile the theoretical models with the observations. Section 6 investigates the intrinsic anisotropy of merger remnants and compares it with their apparent anisotropy, derived from

edge-on projections. A discussion of the results and conclusions follow in section 7.

2 ANALYTICAL CONSIDERATIONS

It is a fundamental stellar dynamical problem to derive the intrinsic dynamical state of a stellar system from its observed projected properties. Binney (1978) used the tensor virial theorem to demonstrate that observed massive, slowly rotating elliptical galaxies are shaped by an anisotropic velocity distribution. Recently, Binney (2005) presented a revised version of his earlier work which properly takes into account projection effects. Here, we shortly summarize the calculations of Binney (2005) which will provide the theoretical basis for the subsequent analysis of the merger remnants. We will restrict ourselves to oblate systems which, as shown below, describe well the geometry of disk, unequal mass merger remnants.

Consider an axisymmetric, oblate stellar system with density distribution $\rho(\vec{x})$. The lengths of the semi-axes of its equidensity surfaces are denoted as a_i . If the x-y-plane is the equatorial plane, $a_x = a_y$ and $a_z < a_x$. We assume that the dominant mean stellar motion is rotation around the z-axis. The equilibrium state of the system is completely determined by the stellar phase space distribution function $f(\vec{x}, \vec{v}) d^3x d^3v$ which denotes the number of stars at location \vec{x} with velocity \vec{v} in the phase space volume $d^3x d^3v$. Given f , the density of stars at \vec{x} is given by

$$\rho(\vec{x}) = \int f d^3v \quad (2)$$

and the mean stellar streaming velocity in the i-th direction is

$$\bar{v}_i(\vec{x}) = \frac{1}{\rho} \int v_i f d^3v. \quad (3)$$

The local velocity dispersion in the i-th direction is

$$\sigma_i^2(\vec{x}) = \frac{1}{\rho} \int (v_i - \bar{v}_i)^2 f d^3v. \quad (4)$$

For oblate systems $\sigma_x = \sigma_y \neq \sigma_z$. We now can define the anisotropy δ of the system

$$\delta \equiv \frac{\Pi_{xx} - \Pi_{zz}}{\Pi_{xx}} \quad (5)$$

where the

$$\Pi_{ii} \equiv \int \rho \sigma_i^2 d^3x \quad (6)$$

are the diagonal elements of the velocity dispersion tensor Π_{ij} . In the isotropic case $\delta = 0$ and $\Pi_{xx} = \Pi_{yy} = \Pi_{zz}$.

Stellar systems are observed in projection. The most ideal situation is the case of an edge-on system where the line-of-sight is parallel to the equatorial plane (x-y plane). In the following we will assume that the y-axis is in the direction of the line-of-sight. Spectroscopic observations then allow a measurement of the mass weighted projected velocity field

$$\bar{v}_{los}(x, z) = \frac{1}{\Sigma} \int \int v_y f d^3v dy \quad (7)$$

and the mass weighted projected velocity dispersion

$$\sigma_{los}^2(x, z) = \overline{v_{los}^2}(x, z) - \bar{v}_{los}^2(x, z). \quad (8)$$

where

$$\overline{v_{los}^2}(x, z) = \frac{1}{\Sigma} \int \int v_y^2 f \, d^3 v \, dy \quad (9)$$

is the mean-square line-of-sight velocity and

$$\Sigma(x, z) = \int \rho \, dy \quad (10)$$

is the surface density at (x, z) .

Two characteristic, global kinematical observables can now be defined that describe the kinematical state of the system: the mean-squared ordered motion

$$\langle \bar{v}_{los}^2 \rangle = \frac{1}{M} \int \int \Sigma \bar{v}_{los}^2 \, dx \, dz \quad (11)$$

and the mean squared velocity dispersion

$$\langle \sigma_{los}^2 \rangle = \frac{1}{M} \int \int \Sigma \sigma_{los}^2 \, dx \, dz. \quad (12)$$

where

$$M = \int \int \Sigma \, dx \, dz \quad (13)$$

is the total mass of the system.

Binney (2005) uses the virial theorem to derive a relationship between these parameters and the anisotropy δ :

$$\left(\frac{v}{\sigma}\right)_{2d}^2 \equiv \frac{\langle \bar{v}_{los}^2 \rangle}{\langle \sigma_{los}^2 \rangle} = \frac{(1-\delta)W_{xx}/W_{zz} - 1}{\alpha(1-\delta)W_{xx}/W_{zz} + 1}, \quad (14)$$

where

$$\alpha = \frac{1}{M \langle \bar{v}_{los}^2 \rangle} \int u^2 \rho \, d^3 x \quad (15)$$

measures the shear in the stellar streaming velocity and

$$u(\vec{x}) = \bar{v}_y(\vec{x}) - v_{los}(x, z) \quad (16)$$

is the difference between the streaming velocity parallel to the line-of-sight at position \vec{x} and the mean projected line-of-sight velocity v_{los} at (x, z) . W_{ii} is a diagonal element of the potential energy tensor. When a system's equidensity surfaces are similar ellipsoids, W_{xx}/W_{zz} depends only on its eccentricity $\epsilon = (1 - a_z/a_x)$, independent of the density distribution ρ (Roberts 1962, Binney 1978)

$$\frac{W_{xx}}{W_{zz}} \equiv q(e) = \frac{0.5}{1 - e^2} \times \frac{\arcsin e - e\sqrt{1 - e^2}}{\frac{e}{\sqrt{1 - e^2}} - \arcsin e} \quad (17)$$

with

$$e = (1 - (1 - \epsilon)^{1/2}). \quad (18)$$

The solid lines in Fig. 1 (which we will call the anisotropy diagram) show the relationship between $(v/\sigma)_{2d}$ and ϵ for different values of δ , adopting $\alpha = 0$. The larger (v/σ) and the larger δ , the larger the ellipticity.

In principle, the equations (11) - (18) can be used to determine the anisotropy of oblate stellar systems from 2-dimensional spectroscopic observations (Emsellem et al. 2004, de Zeeuw et al. 2002). In reality however, inclination effects need to be taken into account (Binney & Tremaine 1987). If ϑ denotes the angle between the system's equatorial plane and the line of sight, the inclined values are

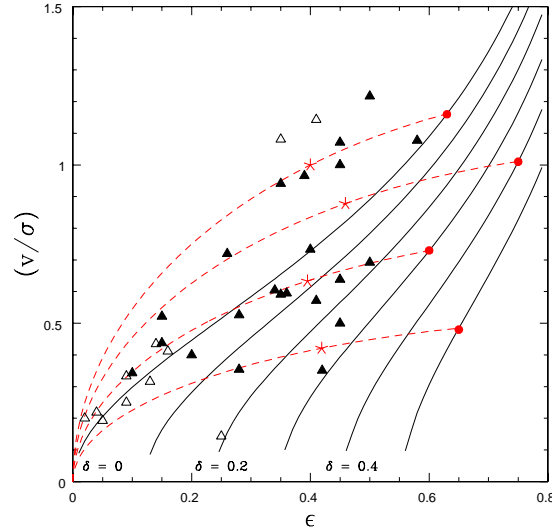


Figure 1. The anisotropy diagram. Solid lines show $(v/\sigma)_{2d}$ versus ϵ for a given anisotropy δ , adopting $\alpha = 0$. Red dashed curves show the effect of inclination for systems which for edge-on projections ($\vartheta = 0$) are located at the red filled points at the right end of each curve. Red stars indicate the locations for an inclination angle of $\vartheta = 30^\circ$. Filled and open triangles show $(v/\sigma)_{1d}$ versus ϵ of observed disk ellipticals with $a_4 \geq 0.5$ and $0 \leq a_4 \leq 0.5$, respectively.

$$\epsilon_{inc} = 1 - \sqrt{1 - \epsilon(2 - \epsilon) \cos^2 \vartheta} \quad (19)$$

$$\left(\frac{v}{\sigma}\right)_{inc} = \left(\frac{v}{\sigma}\right) \times \frac{\cos \vartheta}{(1 - \delta \sin^2 \vartheta)^{1/2}}. \quad (20)$$

The dashed lines in Fig. 1 show how inclination affects (v/σ) and ϵ . For large $(v/\sigma) > 0.5$ or large δ inclination decreases the observed ellipticity with small changes in (v/σ) as the inclination curves cross the lines of constant δ at a large angle. Even small inclination angles therefore can lead to a significant underestimate of the intrinsic anisotropy. This will be crucial when we compare observations with numerical merger remnants. As an illustration, the stars on each dashed curve show the location for an inclination angle of $\vartheta = 30^\circ$, which is expected on average.

3 COMPARISON WITH OBSERVED ELLIPTICALS

Up to now ellipticals have mainly been observed along their apparent major and minor axis which does not allow us to derive $\langle \bar{v}_{los}^2 \rangle$ or $\langle \sigma_{los}^2 \rangle$, required to determine δ from equation (14). Instead the central line-of-sight velocity dispersion σ_0 and the characteristic peak rotational velocity along the major axis v_{maj} have been used. In this case, δ can be derived from the relation (Binney 1978, 2005)

$$\left(\frac{v}{\sigma}\right)_{1d}^2 \equiv \left(\frac{v_{maj}^2}{\sigma_0^2}\right) = \frac{\pi^2}{8} \left((1 - \delta) \frac{W_{xx}}{W_{zz}} - 1 \right). \quad (21)$$

Equation 21 is very similar to equation (14) for the case of $\alpha = 0$ with the observational errors being much larger than the correction factor ($\pi^2/8$). We therefore will use Fig. 1 to investigate the anisotropy of observed ellipticals.

The filled triangles in Fig. 1 show observed disk elliptical galaxies with $a_4 \geq 0.5$ (Bender, Burstein & Faber 1992). Open triangles represent ellipticals with small values of $0 < a_4 < 0.5$ which populate the lower left corner where the ellipticities and the rotational velocities are small. This would be expected if these galaxies are seen almost face-on ($\vartheta = 90^\circ$) as large inclinations lead to small ϵ and (v/σ) and also significantly reduce the projected a_4 -values. At first, the observations appear to support the standard expectation that disk ellipticals are on average isotropic ($\delta = 0$) and rotationally flattened.

4 THE LOCATION OF MERGER REMNANTS IN THE ANISOTROPY DIAGRAM

Naab & Burkert (2001, 2003) presented a large parameter set of collisionless galaxy mergers. Equilibrium spirals were generated following Hernquist (1993), consisting of an exponential disk, a spherical, non-rotating bulge and a pseudo-isothermal halo. The mass ratios η of the progenitor disks were varied between $\eta = 1$ and $\eta = 4$. The galaxies were assumed to approach each other on nearly parabolic orbits with an initial separation of 30 length units and a pericenter distance of 2 length units, where a length unit is equal to the exponential scale length of the more massive disk galaxy. Free parameters were the inclinations of the two disks relative to the orbital plane and the arguments of pericenter. In order to select an unbiased sample of initial disk orientations the procedure described by Barnes (1988) was applied. In total 16 equal-mass mergers and 96 mergers with $\eta = 2, 3, 4$ were calculated. The merger products were allowed to settle into equilibrium for 10 dynamical timescales.

The remnants were analysed following as closely as possible the procedures of observers as described by Bender (1988a,b). First, an artificial image of the remnant was created by binning the projected remnant into 128×128 pixels. This picture was smoothed with a Gaussian filter of standard deviation 1.5 pixels. The isophotes and their a_4 values were then determined using a data reduction package provided by Ralf Bender. Following the standard definitions of observers, the central projected velocity dispersion σ_0 inside a projected galactocentric distance of 0.2 effective radii, the characteristic ellipticity ϵ , defined as the isophotal ellipticity at 1.5 effective radii and the characteristic rotational velocity v_{maj} , defined as the projected rotational velocity on the major axis at 1.5 effective radii was determined.

A detailed investigation of the intrinsic orbital structure of the merger remnants and their global photometric and kinematical properties has been presented elsewhere (Naab & Burkert 2001, 2003; Jesseit, Naab & Burkert 2005). Here we focus on their anisotropy. Figure 2 shows the location of disk ($a_4 > 0.5$) equal- and unequal mass merger remnants in the anisotropy diagram. Like the observations, we here plot $(v/\sigma)_{1d}$ of the projected systems. The remnants have been rotated such that they are seen edge-on ($\vartheta = 0$) and are analysed with the line-of-sight parallel to their intermediate axis. Almost all unequal-mass mergers are disk. The

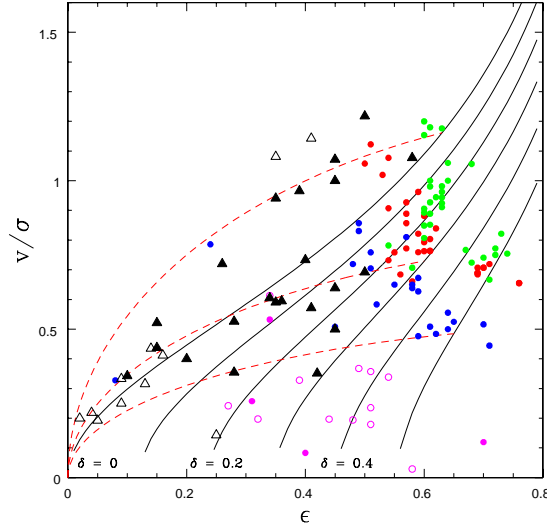


Figure 2. $(v/\sigma)_{1d}$ versus ϵ of edge-on ($\vartheta = 0$) merger remnants in the anisotropy diagram. Green points show 4:1 mergers, red points correspond to 3:1 mergers and blue points are 2:1 mergers. The magenta filled points show disk-like equal-mass merger remnants while magenta open points correspond to boxy equal-mass mergers.

situation is different for equal-mass mergers. Only a few 1:1 mergers produced disk-like remnants (filled magenta points) for edge-on projections. For comparison we also plot the boxy 1:1 mergers as open magenta points.

The disk-like unequal-mass mergers are obviously not isotropic, in contrast to previous claims. They fill the whole region between $\delta = 0$ and $\delta = 0.5$. In fact, our sample contains a larger fraction of anisotropic 4:1 mergers with $\delta \geq 0.4$ than is found for 1:1 mergers. Note also that there are almost no 3:1 to 4:1 mergers with $\delta = 0.3 - 0.4$. This might be due to the still limited coverage of the parameter space of initial disk inclinations. The precise location of a merger remnant in the anisotropy diagram appears to depend critically on the initial disk orientations. We will investigate this interesting sensitivity on the initial conditions in greater details in a subsequent paper. In summary, the main difference between equal and unequal mass merger remnants is not their anisotropy but rather their rotation. Given the anisotropy δ , increasing the mass ratio η will increase the value of (v/σ) . In addition, for a given mass ratio, the more anisotropic the system the smaller its (v/σ) .

Clearly, the observations of disk ellipticals are not in agreement with edge-on merger remnants. One might argue that an additional dissipative gas component could affect the rotation and ellipticity. In order to investigate this question, we calculated all 3:1 mergers again, including now an additional gaseous disk in the progenitors with a mass fraction of 10% the stellar mass. A detailed analyses of these and additional simulations with different gas fractions will be presented in a subsequent paper. Here we just note that the gas has an important effect on the intrinsic orbital structure of the remnants as it prohibits the formation of box orbits,

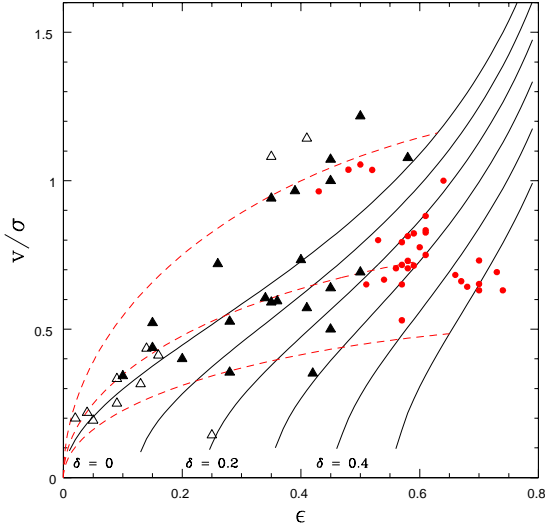


Figure 3. 3:1 merger remnants of disk galaxies are shown. The progenitors, in addition to the stellar component also contained a gaseous disk with a gas-to-star mass fraction of 10%.

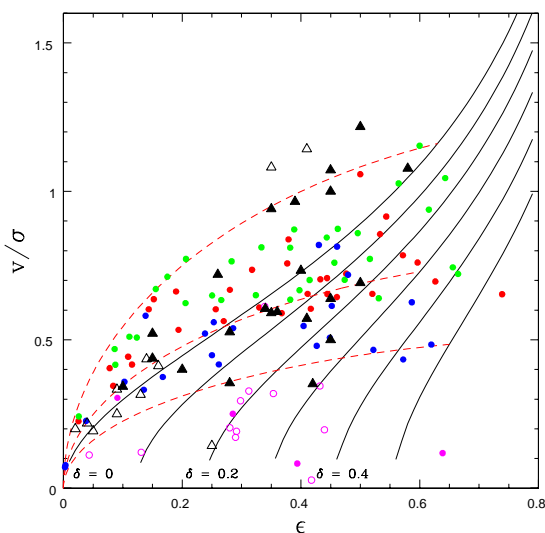


Figure 4. The distribution of projected merger remnants is compared with observed disk ellipticals. The symbols are explained in Fig. 2.

by this also affecting the shape of the observable line-of-sight velocity distribution. However, somewhat surprisingly, the distribution of the merger remnants in the anisotropy diagram is not affected as is shown in Fig. 3.

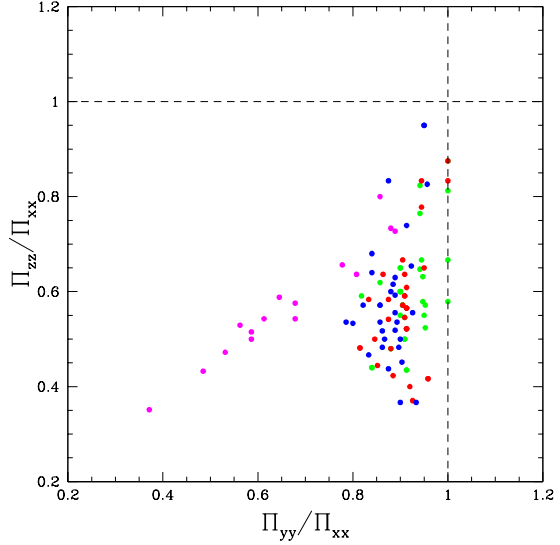


Figure 5. The ratios of the diagonal elements of the velocity dispersion tensor are shown for equal- and unequal-mass merger remnants. The symbols are described in Fig. 2.

5 INCLINATION EFFECTS

As mentioned earlier, inclination effects can efficiently decrease the apparent anisotropy of fast rotating ellipticals. The dashed lines in Fig. 2 show that inclining the merger remnants would indeed move them into the region occupied by the observations. To investigate this effect more quantitatively, Fig. 4 shows again the distribution of the merger remnants in the anisotropy diagram, however now inclined with respect to the line-of-sight. For each object an inclination angle ϑ was randomly chosen with a probability $p(\vartheta) d\vartheta = \sin \vartheta d\vartheta$. With a few exceptions, the distribution of merger remnants is in very good agreement with the observations. It might be interesting to note that the observed ellipticals appear to cluster in two groups. Group 1 is fast rotating with $(v/\sigma) \approx 1$. This group can be barely fitted even by 4:1 merger remnants (Naab & Burkert 2003, Cretton et al. 2001). Group 2 is characterized by $0.4 \leq (v/\sigma) \leq 0.7$ and can be well explained by inclined 2:1 - 4:1 mergers. 1:1 mergers are rotating too slowly to fit disk ellipticals, independent of inclination.

6 THE INTRINSIC ANISOTROPY OF FAST ROTATING MERGER REMNANTS

Is the anisotropy δ as derived from equation 21, using the observables v_{maj} , σ_0 and ϵ a good estimate of the intrinsic anisotropy of fast rotating stellar systems? To investigate this question, we have calculated the diagonal components Π_{ii} of the intrinsic velocity dispersion tensor (equation 6) of our merger remnants. Figure 5 shows the relation between the ratios of the diagonal elements for all mergers. In agreement with our previous assumption $\Pi_{xx} \approx \Pi_{yy} > \Pi_{zz}$ for

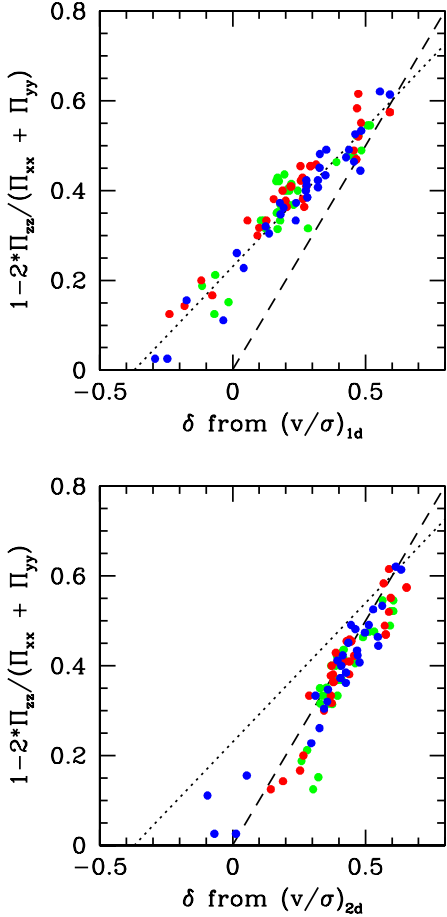


Figure 6. The upper panel compares the anisotropy δ of edge-on unequal-mass merger remnants, calculated from the projected central velocity dispersion, characteristic major axis rotation and characteristic ellipticity (equ. 21) with their intrinsic anisotropy. The dotted line shows a fit through the data (eq. 22). The lower panel compares the intrinsic anisotropy with δ , derived from equation 14 using the mean-squared ordered motion and velocity dispersion of the projected, edge-on system and adopting $\alpha = 0$. The symbols are described in Fig. 2.

unequal mass remnants. In contrast, boxy equal-mass mergers are characterized by $\Pi_{xx} > \Pi_{yy} \approx \Pi_{zz}$.

Let us define the intrinsic anisotropy of an oblate merger remnant as $1 - 2\Pi_{zz}/(\Pi_{xx} + \Pi_{yy})$. The upper panel of Fig. 6 compares this quantity with the "observationally" determined anisotropy δ , derived from $(v/\sigma)_{1d}$ (Eq. 21). The dashed curve shows the correlation expected if both variables would agree. The merger remnants have on average larger intrinsic anisotropies than inferred from the projected properties. The deviation increases with decreasing δ . Those ellipticals that appear isotropic actually have an intrinsic anisotropy of 0.2, while ellipticals with apparently negative values of $\delta \approx -0.3$ are in reality isotropic.

The knowledge of just three characteristic parameters $(v_{maj}, \sigma_0, \epsilon)$ therefore seems not to be sufficient to determine

the intrinsic anisotropy of disk ellipticals accurately. One possible improvement is the spectroscopic measurement of the two-dimensional projected average velocity field $\bar{v}_{los}(x, z)$ and the two-dimensional projected distribution of the velocity dispersion $\sigma_{los}^2(x, z)$. From this the mean-squared ordered motion $\langle \bar{v}_{los}^2 \rangle$ (eq. 11) and the mean squared velocity dispersion $\langle \sigma_{los}^2 \rangle$ (eq. 12) could be derived and, given ϵ , equation (14) leads to a more precise determination of δ . A crucial and uncertain parameter is the value of α which Binney (2005) estimates to be of order 0.13. We have calculated the α of our merger remnants and find values of order 0.08 to 0.2 for 3:1 and 4:1 remnants with somewhat larger values for 2:1 mergers. α tends to increase with decreasing (v/σ) and decreasing progenitor mass ratio η . However the total number of particles used in our simulations is too small to determine α accurately and simulations with substantially larger particle numbers would be required. Interestingly, using $\alpha = 0$ already leads to a reasonably good estimate of the intrinsic anisotropy. To demonstrate this, the lower panel of Fig. 6 plots δ , derived from $(v/\sigma)_{2d}$ with $\alpha = 0$, using equation 14 and compares it with the intrinsic anisotropy of the merger remnants. The agreement is much better than previously.

The upper panel of Fig. 6 shows that all fast rotating, disk ellipticals follow a narrow correlation between the intrinsic and observationally inferred anisotropy which can be well fitted by the empirical formula (dotted line)

$$1 - 2\Pi_{zz}/(\Pi_{xx} + \Pi_{yy}) = 0.62 \delta + 0.23. \quad (22)$$

This suggests a second, less expensive method to determine the intrinsic anisotropy from the usually measured observables: ϵ , σ_0 and v_{maj} . Using equation 21, a first estimate of δ is derived. Equation 22 then gives the intrinsic anisotropy. Note however that all of these considerations require first a correction due to inclination. Unless the inclination angle ϑ of the system is known, e.g. by measuring the orientation of an additional central disk component, inclination effects will dominate the uncertainties and will make a precise determination of the intrinsic anisotropy impossible.

7 CONCLUSIONS

Numerical simulations of unequal-mass disk galaxy mergers lead to fast rotating stellar systems that resemble observed disk elliptical galaxies. However, in contrast to previous claims, the objects have a large spread in their anisotropies, ranging from almost isotropic systems to objects with $1 - \Pi_{zz}/(\Pi_{xx} + \Pi_{yy}) \approx 0.65$. The distribution of anisotropies is similar to boxy, slowly rotating merger remnants that result from equal-mass mergers and that are believed to explain the origin of massive boxy ellipticals. The main difference between disk and boxy ellipticals therefore is not anisotropy but the amount of rotation and the fact that unequal-mass mergers are characterised by $\Pi_{xx} \approx \Pi_{yy} > \Pi_{zz}$ whereas equal-mass mergers have $\Pi_{xx} > \Pi_{yy} \approx \Pi_{zz}$.

Figure 2 shows that the ellipticity of anisotropic fast rotating merger remnants is larger than expected for the isotropic case which means that the flattening of these objects is at least partly a result of their anisotropic velocity distribution. Including gas does not change this conclusion. For example, 3:1 and 4:1 merger remnants with

$\delta \approx 0.5$ and $v/\sigma \approx 0.7$ have ellipticities of $\epsilon \approx 0.7$, whereas isotropic objects with similar values of v/σ would be much rounder with $\epsilon \approx 0.4$. Inclination effects strongly reduce the apparent anisotropy, especially for fast rotating systems. For example, Fig. 1 shows that objects with $v/\sigma \approx 1$ and $\delta = 0.5$ would already appear isotropic with $\delta = 0$ when viewed under an inclination angle of $\vartheta = 30^\circ$. This explains why fast rotating disk ellipticals appear isotropic and reconciles the predictions of the major merger scenario with the observations. Clearly, more work on determining inclination angles for fast rotating ellipticals is required to gain a deeper insight into their internal dynamical structure and their origin.

We thank James Binney for sharing his new analytical calculations on the anisotropy determination of projected stellar systems with us prior to publication. We also thank Ralf Bender for many interesting discussions.

REFERENCES

- Barnes, J. E. 1988, ApJ, 331, 699
 Barnes, J. E. 1998, Saas-Fee Advanced Course 26: Galaxies: Interactions and Induced Star Formation, 275
 Bekki, K. 1999, ApJ, 513, 108
 Bender, R. 1988a, A&A, 193, L7
 Bender, R. 1988b, A&A, 202, L5
 Bender, R., Surma, P., Doebeleiner, S., Moellenhoff, C., & Madejsky, R. 1989, A&A, 217, 35
 Bender, R., Burstein, D., & Faber, S. M. 1992, ApJ, 399, 462
 Bendo, G.J. & Barnes, J.E. 2000, MNRAS, 316, 315
 Binney, J. 1978, MNRAS, 183, 779
 Binney, J. 1985, MNRAS, 212, 767
 Binney, J. & Tremaine, S. 1987, Galactic Dynamics, Princeton University Press
 Binney, J. 2005, astro-ph/0504387
 Bournaud, J., Combes, F. & Jog, C.J. 2004, A & A, 418, 27
 Burkert, A. & Naab, T. 2004a, in 'Galaxies and Chaos', eds. G. Contopoulos & N. Voglis, Lecture Notes in Physics (Springer), p. 327
 Burkert, A. & Naab, T. 2004b, in 'Coevolution of Black Holes and Galaxies', ed. L.C. Ho, Cambridge Univ. Press, p. 422
 Cretton, N., Naab, T., Rix, H.W. & Burkert, A. 2001, ApJ, 554, 291
 Cox, T.J., Jonsson, P., Primack, J.R. & Somerville, R.S. 2005, submitted to MNRAS (astro-ph/0503201)
 Dehnen, W. & Gerhard, O.E. 1994, MNRAS, 268, 1019
 De Zeeuw, P.T. et al. 2002, MNRAS, 329, 513
 Di Matteo, T., Springel, V. & Hernquist, L. 2005, Nature, 433, 604
 Emsellem, E. et al. 2004, MNRAS, 352, 721
 Ferrarese, L. & Merritt, D. 2000, ApJ, 539, L9
 Gebhardt, K. et al. 2000, ApJ, 539, L13
 Gerhard, O.E. 1981, MNRAS, 197, 179
 González-García, A.C. & van Albada, T.S. 2003, MNRAS, 342, 36
 González-García, A.C. & Balcells, M. 2005, MNRAS, 357, 753
 Hernquist, L. 1992, ApJ, 400, 460
 Hernquist, L. 1993, ApJ, 409, 548
 Jesseit, R., Naab, T. & Burkert, A. 2005, MNRAS, in press (astro-ph/0501418)
 Khochfar, S. & Burkert, A. 2005, MNRAS, in press (astro-ph/0409705)
 Merrifield, M.R. 2004, MNRAS, 353, 13
 Meza, A., Navarro, J.F., Steinmetz, M. & Eke, V.R. 2003, ApJ, 590, 619
 Mihos, J.C. & Hernquist, L. 1996, ApJ, 464, 641
 Naab, T., Burkert, A., & Hernquist, L. 1999, ApJL, 523, L133
 Naab, T. & Burkert, A. 2001, ApJL, 555, L91
 Naab, T. & Burkert, A. 2003, ApJ, 597, 893
 Negroponte, J. & White, S.D.M. 1983, MNRAS, 205, 1009
 Nipoti, C., Londrillo, P. & Ciotti, L. 2003, MNRAS, 342, 501
 Roberts, P.H. 1962, ApJ, 136, 1108
 Searle, L., Sargent, W.L.W. & Bagnuolo, W.G. 1973, ApJ, 179, 427
 Springel, V., Di Matteo, T. & Hernquist, L. 2005, ApJ, 620, L79
 Toomre, A. & Toomre, J. 1972, ApJ, 178, 623
 Tremaine, S., et al. 2002, ApJ, 574, 740
 Trujillo, I., Erwin, P., Asensio Ramos, A. & Graham, A.W. 2004, AJ, 127, 1917